**Supporting Information**

# Theoretical Study of 2D Polymeric $C_{24}$ Networks as High-Performance Anchoring Materials for Lithium-Sulfur Batteries

Jiguang Du[1,*], Jiahao Deng[1,2], Mingyang Shi[1,2], Gang Jiang[2]

[1]*College of Physics, Sichuan University, Chengdu 610065, China*

[2]*Institute of Atomic and Molecular Physics, Sichuan University, Chengdu 610065, China*

## Table of contents



* E-mail: dujg@scu.edu.cn

**Complement to Computational Detail**

The sulfur reduction reaction (SRR) in the discharging process is expressed as follows,

$$S_8 + 16Li^+ \ (Na^+) + 16e^- = 8Li_2S \ (Na_2S)$$

The elementary step involved in the generation of one $Li_2S$ molecule is as follows,

$$* S_8 + 2Li^+ (Na^+) + 2e^- = * Li_2S_8 (* Na_2S_8)$$

$$* Li_2S_8 (* Na_2S_8) = * Li_2S_6 (* Na_2S_6) + 1/4 \ S_8$$

$$* Li_2S_6 (* Na_2S_6) = * Li_2S_4 (* Na_2S_4) + 1/4 \ S_8$$

$$* Li_2S_4 (* Na_2S_4) = * Li_2S_2 (* Na_2S_2) + 1/4 \ S_8$$

$$* Li_2S_2 (* Na_2S_2) = * Li_2S (* Na_2S) + 1/8 \ S_8$$

wherein * is the active site on the substrate.

The reaction Gibbs free energy of each step is calculated with the following equation:

$$\Delta G = \Delta E + \Delta E_{ZPE} - T\Delta S \qquad \text{(S1)}$$

where $\Delta E$ represents the adsorption energy, $\Delta E_{ZPE}$ and $T\Delta S$ denote the zero-point energy difference and entropy difference between the products and reactants obtained from the frequency calculations at 298.15 K.

Table S1. Calculated lattice parameters of $C_{24}$ monolayers and bilayers in both phases,

cohesive energies per atom ($E_c$), and additional cohesive energy for monolayer formation from molecules ($\Delta E_c$) of both $C_{24}$ phases, and binding energy ($E_b$) of bilayer $C_{24}$ in both phases.

| | $a$ (Å) | $b$ (Å) | $E_{gap}$ (eV) | $E_c$ (eV/atom)[a] | $\Delta E_c$ (eV/atom[b] | $E_b$ (meV/atom)[c] |
|---|---|---|---|---|---|---|
| qHP $C_{24}$ monolayer | 11.532 | 6.198 | 3.04 | −9.434 | −0.391 | |
| | (11.500)[d] | (6.180)[d] | 3.10 | (−8.974)[d] | (−0.388)[d] | |
| qTP $C_{24}$ monolayer | 6.123 | 6.123 | 3.75 | −9.371 | −0.328 | |
| | (6.103)[d] | (6.103)[d] | 3.74 | (−8.914)[d] | (−0.328)[d] | |
| qHP $C_{24}$ bilayer | 11.526 | 6.198 | 3.00 | | | −15.64 |
| qTP $C_{24}$ bilayer | 6.122 | 6.121 | 3.55 | | | −15.61 |

[a]The $E_c$ values were calculated with the following equation: $E_c = E$ (monolayer)/n – $E$ (atom), where $E$ (monolayer) is the energy of the monolayer per unit cell, n is the number of C atoms in the unit cell, and $E$ (atom) is the energy of an isolated C atom.

[b]The $\Delta E_c$ values were calculated with the following equation: $\Delta E_c = [E$ (monolayer) – m$E$ ($C_{24}$)]/n, where $E$ (monolayer) is the energy of the monolayer per unit cell, m and n are the number of $C_{24}$ clusters and C atoms in the unit cell, and $E$ ($C_{24}$) is the energy of an isolated $C_{24}$ cluster.

[c]The $E_b$ values were calculated with the following equation: $E_b = [E$ (bilayer) – 2$E$ (monolayer)]/n, where $E$ (bilayer) and $E$ (monolayer) are the energy of the bilayer and monolayer per unit cell, respectively, n is the number of C atoms in the monolayer unit cell.

[d]The values reported in previous work[1] are shown in parentheses for comparison.

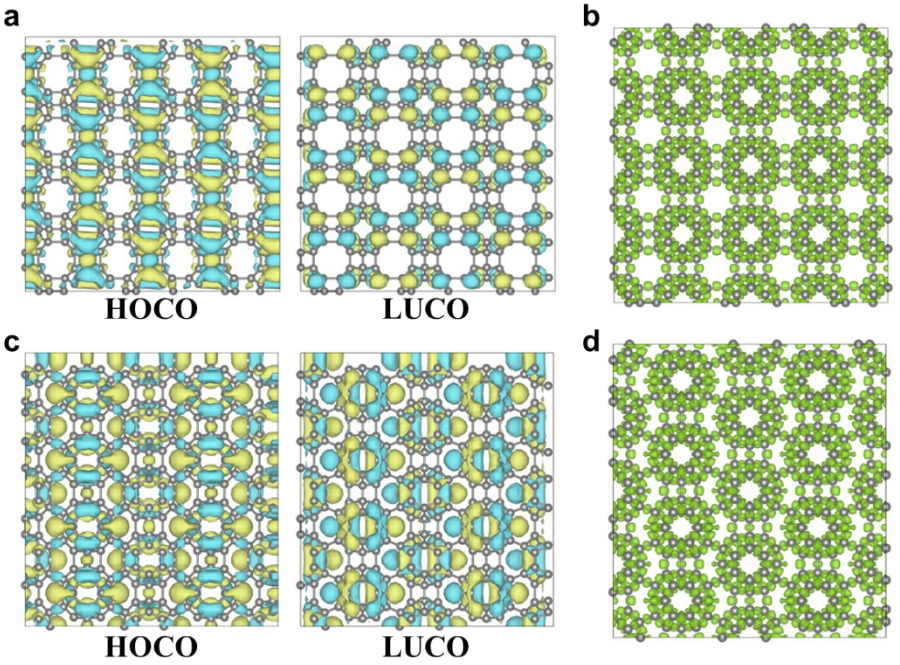


Figure S1. Top view of the HOCO and LUCO isosurfaces (isovalue = 0.008) for monolayer networks, qHP (a), qTP (c). Top view of the ELF isosurfaces (isovalue = 0.8) for monolayer networks, qHP (b), qTP (d). The C atoms are represented by gray spheres.

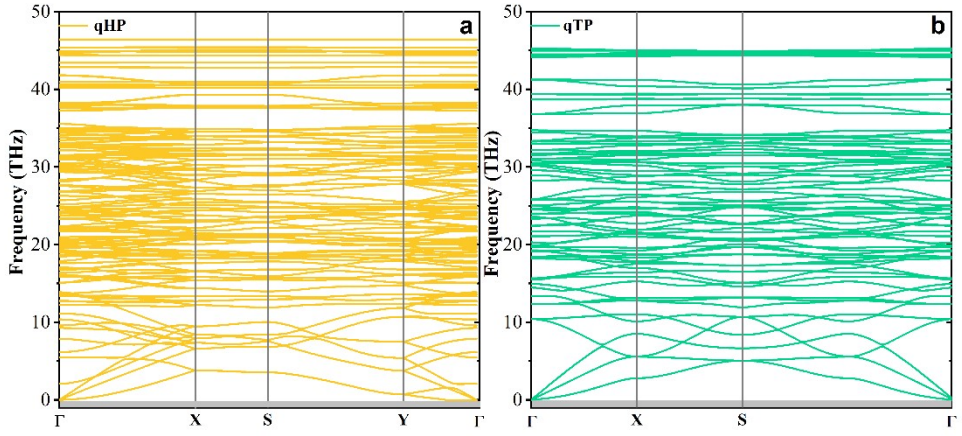


Figure S2. Phonon dispersion curves of qHP (a) and qTP (b) $C_{24}$ monolayers.

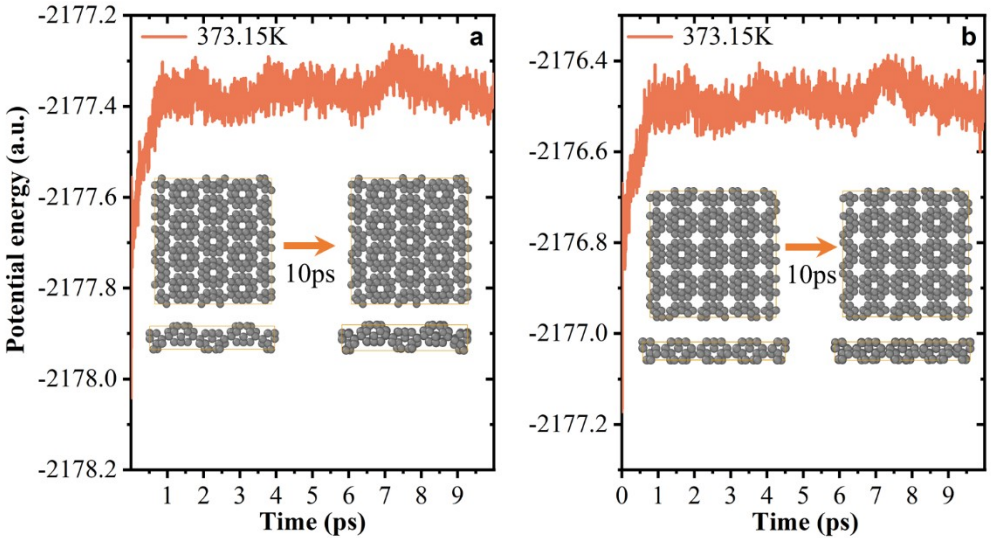


Figure S3. Fluctuation of potential energy at 373.15 K for qHP (a) and qTP (b) $C_{24}$ monolayers. The snapshots at 0 ps and 10 ps are inserted. The C atoms are represented by gray spheres.

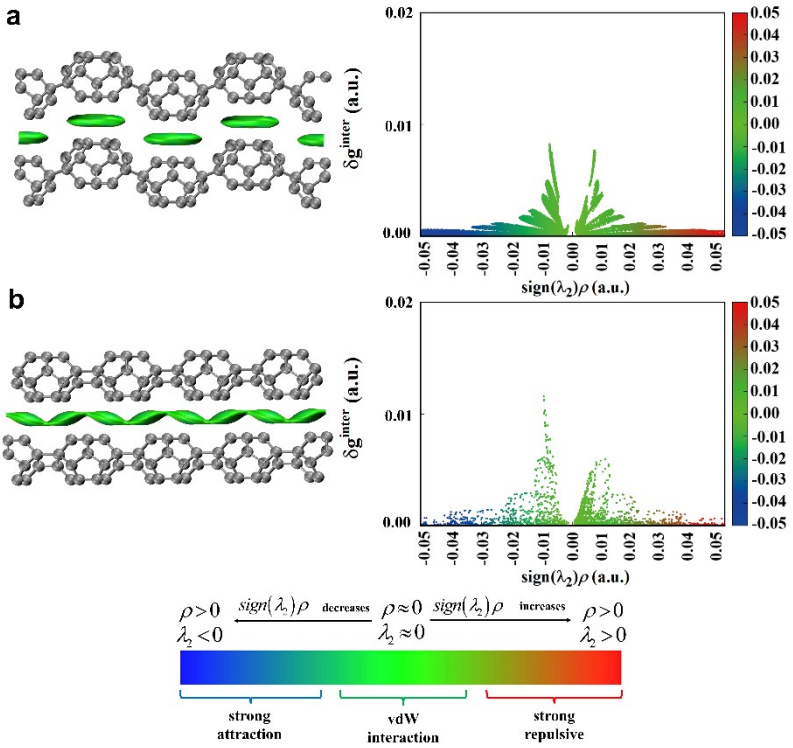


Figure S4. Color-filled independent gradient model (IGM) isosurface (isovalue = 0.002) (left) and scatter plots (right) depicting average noncovalent interaction regions for qHP (a) and qTP (b) $C_{24}$ bilayers. In the IGM, the blue patches represent attractive interactions, green patches indicate van der Waals forces, and red patches depict repulsive interactions. The C atoms are represented by gray spheres.

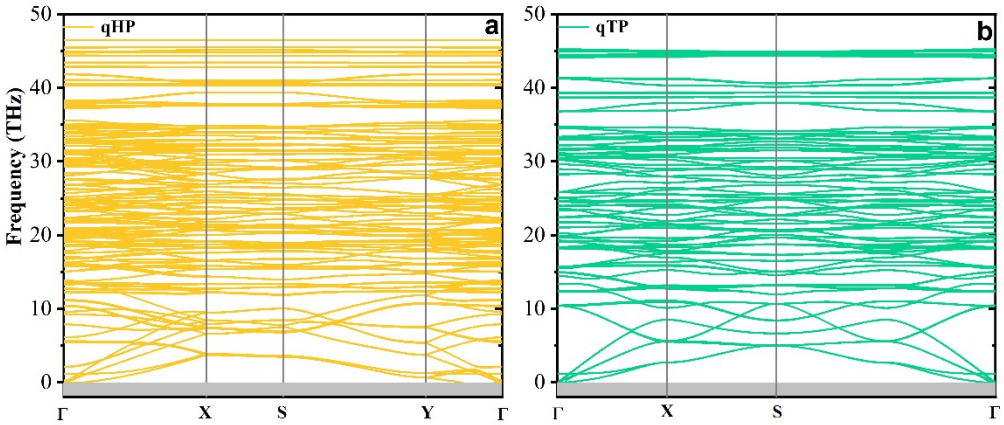


Figure S5. Phonon dispersion curves of qHP (a) and qTP (b) $C_{24}$ bilayers.

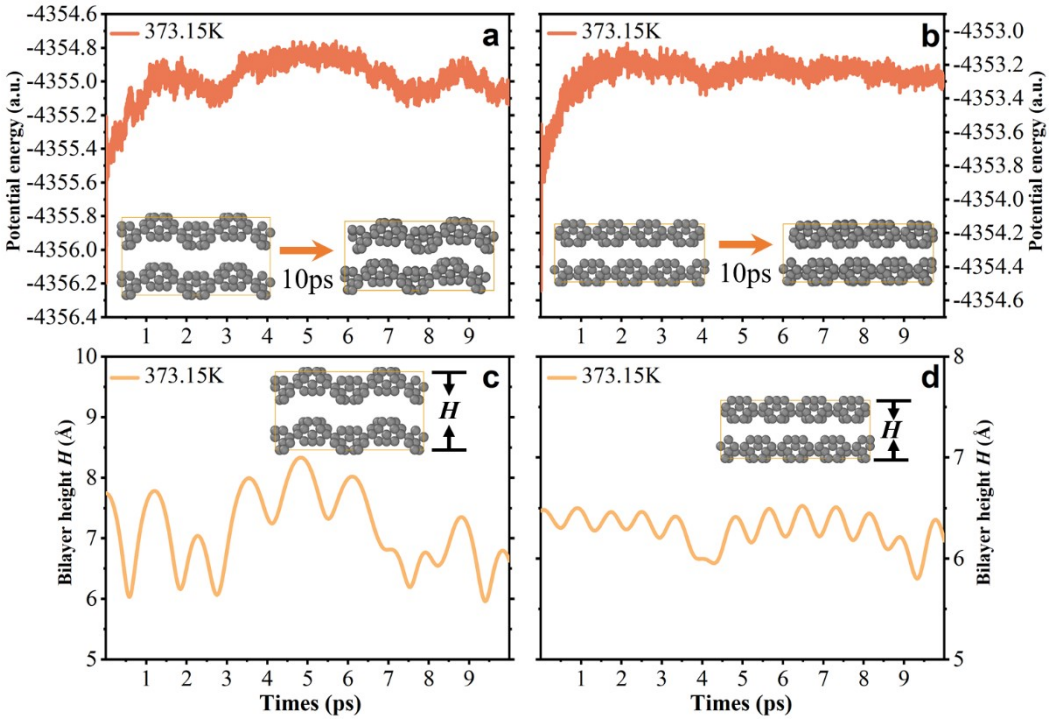


Figure S6. Fluctuation of potential energy at 373.15 K for qHP (a) and qTP (b) $C_{24}$ bilayers. The snapshots at 0 ps and 10 ps are inserted. Fluctuation of interlayer heights for qHP (c) and qTP (d) $C_{24}$ bilayers. The C atoms are represented by gray spheres.

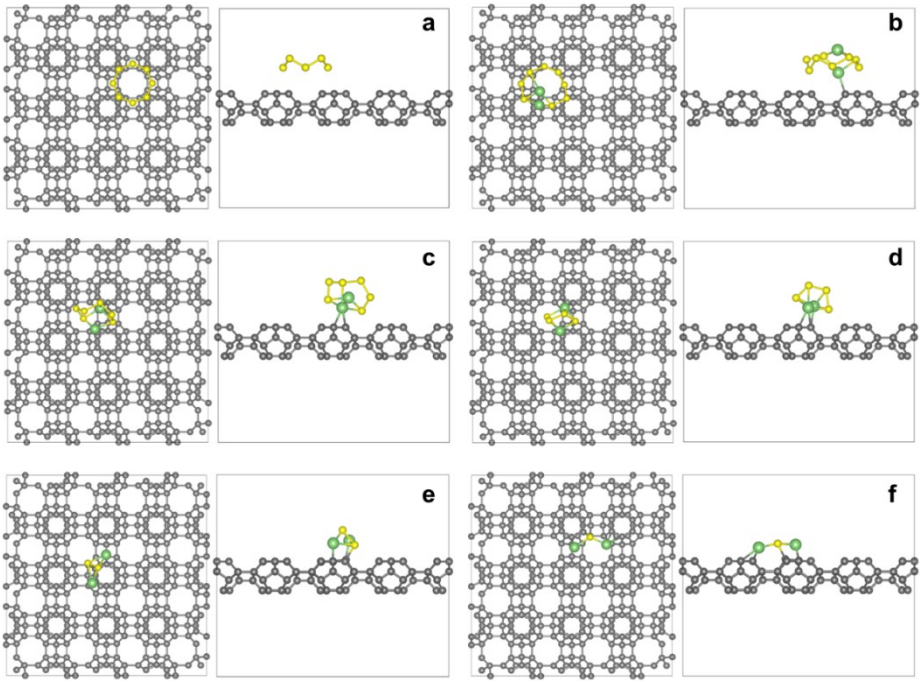


Figure S7. Relaxed configurations of qTP $C_{24}$ monolayers with adsorptions of $S_8$ (a), $Li_2S_8$ (b), $Li_2S_6$ (c), $Li_2S_4$ (d), $Li_2S_2$ (e), and $Li_2S$ (f). The C, S, and Li atoms are represented by gray, yellow, and green spheres, respectively.

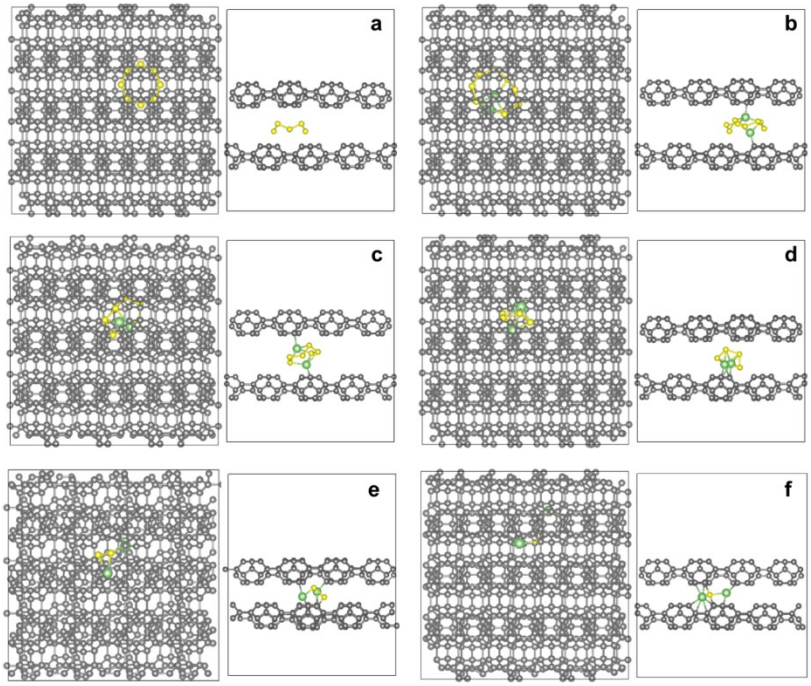


Figure S8. Relaxed configurations of qTP $C_{24}$ bilayers with adsorptions of $S_8$ (a), $Li_2S_8$ (b), $Li_2S_6$ (c), $Li_2S_4$ (d), $Li_2S_2$ (e), and $Li_2S$ (f). The C, S, and Li atoms are represented by gray, yellow, and green spheres, respectively.

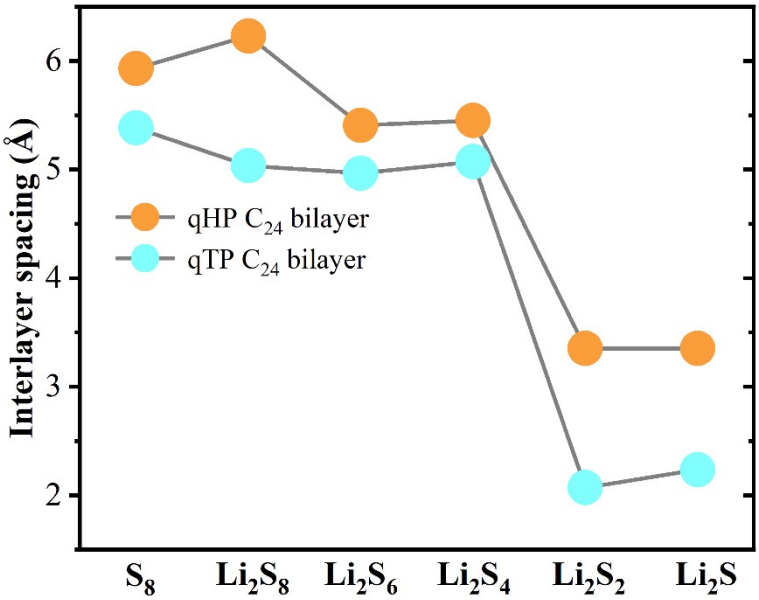


Figure S9. Interlayer spacing of qHP and qTP $C_{24}$ bilayers with adsorptions of $S_8$ and $Li_2S_x$ clusters.

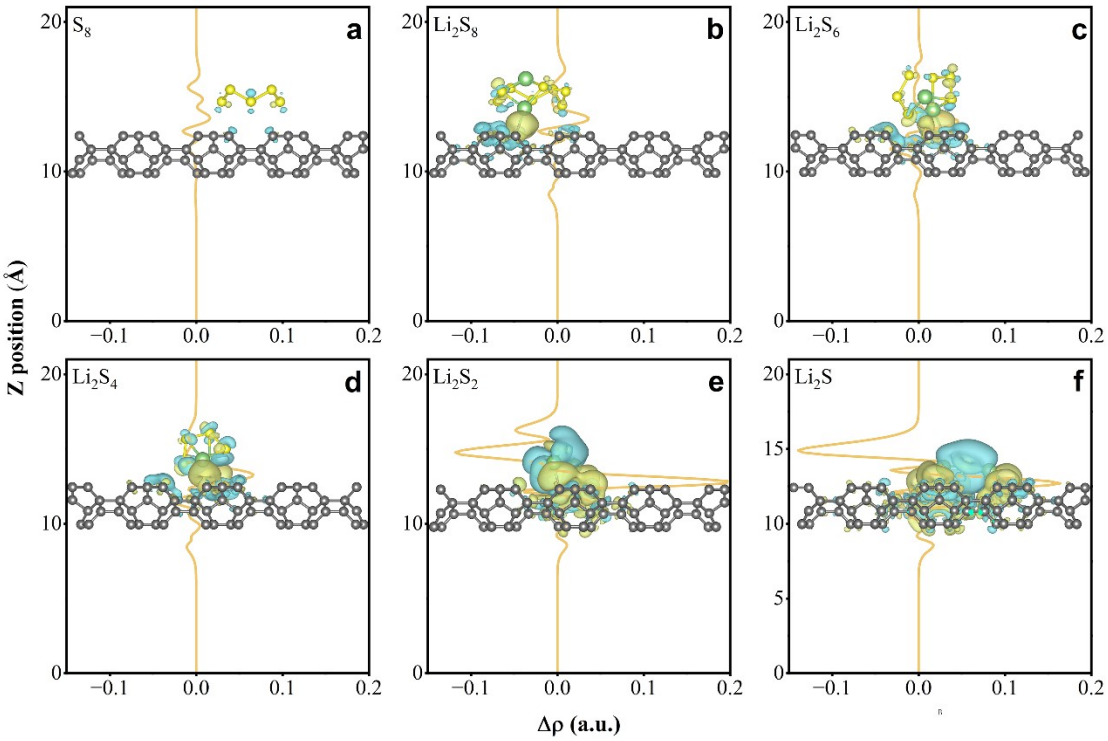


Figure S10. Plane averaged charge density differences (CDD) of the qTP $C_{24}$ monolayer with adsorptions of $S_8$ (a), $Li_2S_8$ (b), $Li_2S_6$ (c), $Li_2S_4$ (d), $Li_2S_2$ (e), $Li_2S$ (f), positive values represent electron accumulation, and negative values indicate electron depletion. The CDD isosurfaces (isosurface = 0.005 a.u.) are also illustrated in the background of the figure, the cyan and yellow regions of the charge density difference represent charge loss and charge aggregation, respectively. The C, S, and Li atoms are represented by gray, yellow, and green spheres, respectively.

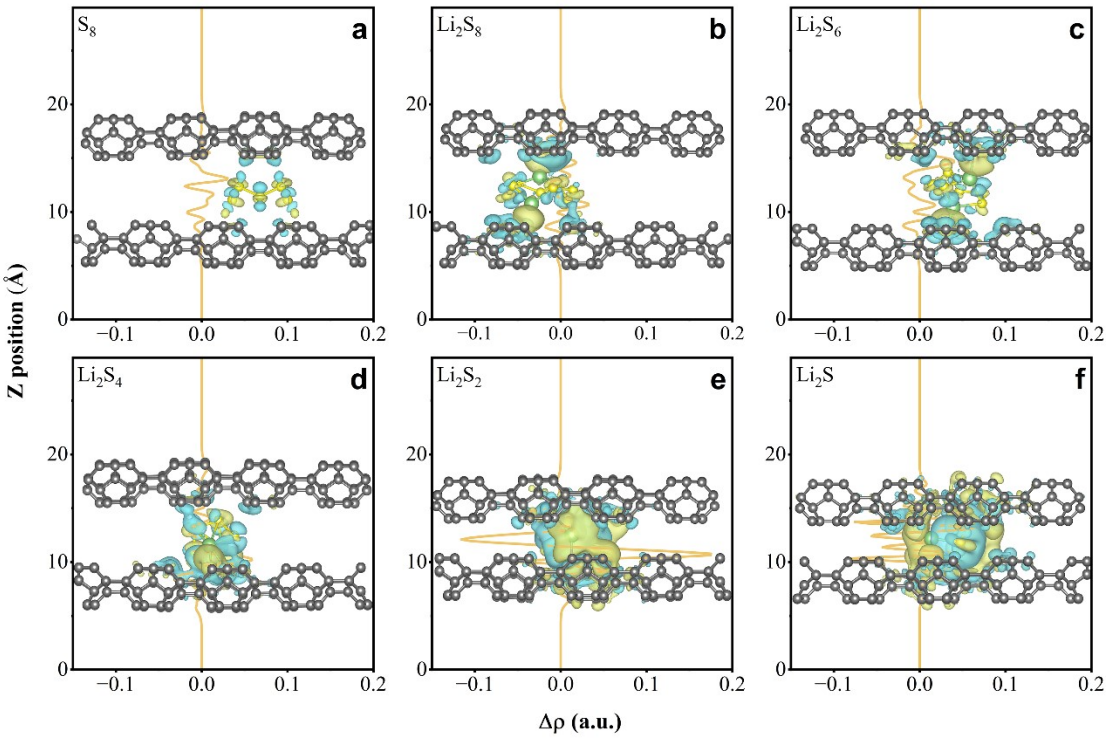


Figure S11. Plane averaged charge density differences (CDD) of the qTP $C_{24}$ bilayer with adsorptions of $S_8$ (a), $Li_2S_8$ (b), $Li_2S_6$ (c), $Li_2S_4$ (d), $Li_2S_2$ (e), $Li_2S$ (f), positive values represent electron accumulation, and negative values indicate electron depletion. The CDD isosurfaces (isosurface = 0.005 a.u.) are also illustrated in the background of the figure, the cyan and yellow regions of the charge density difference represent charge loss and charge aggregation, respectively. The C, S, and Li atoms are represented by gray, yellow, and green spheres, respectively.

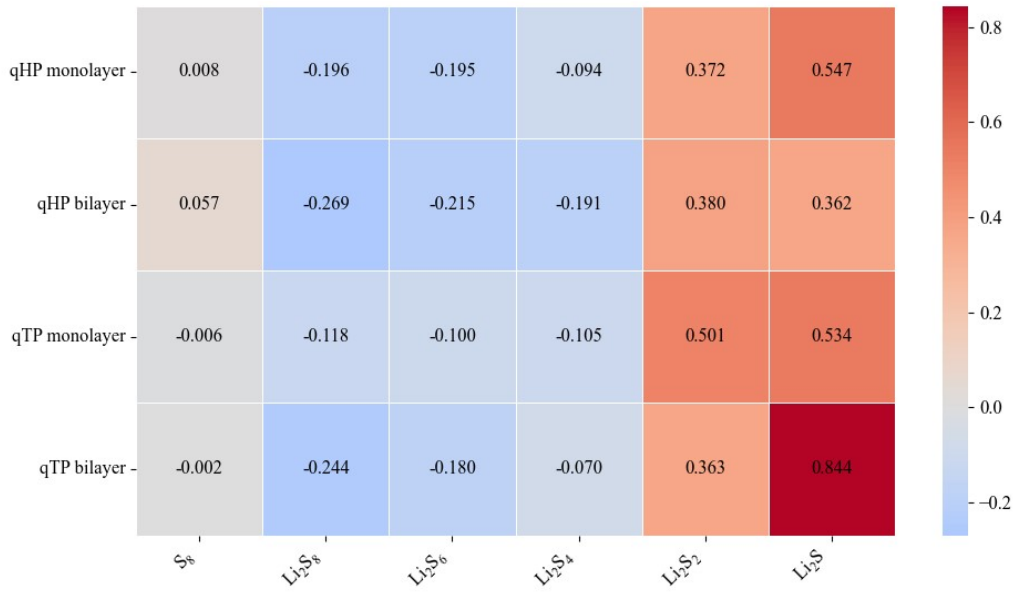


Figure S12. Charge transfers (ΔQ) from adsorbates ($S_8$ and LiPSs) to the $C_{24}$ monolayers and bilayers. Positive ΔQ values indicate that electrons are transferred from adsorbates to substrates.

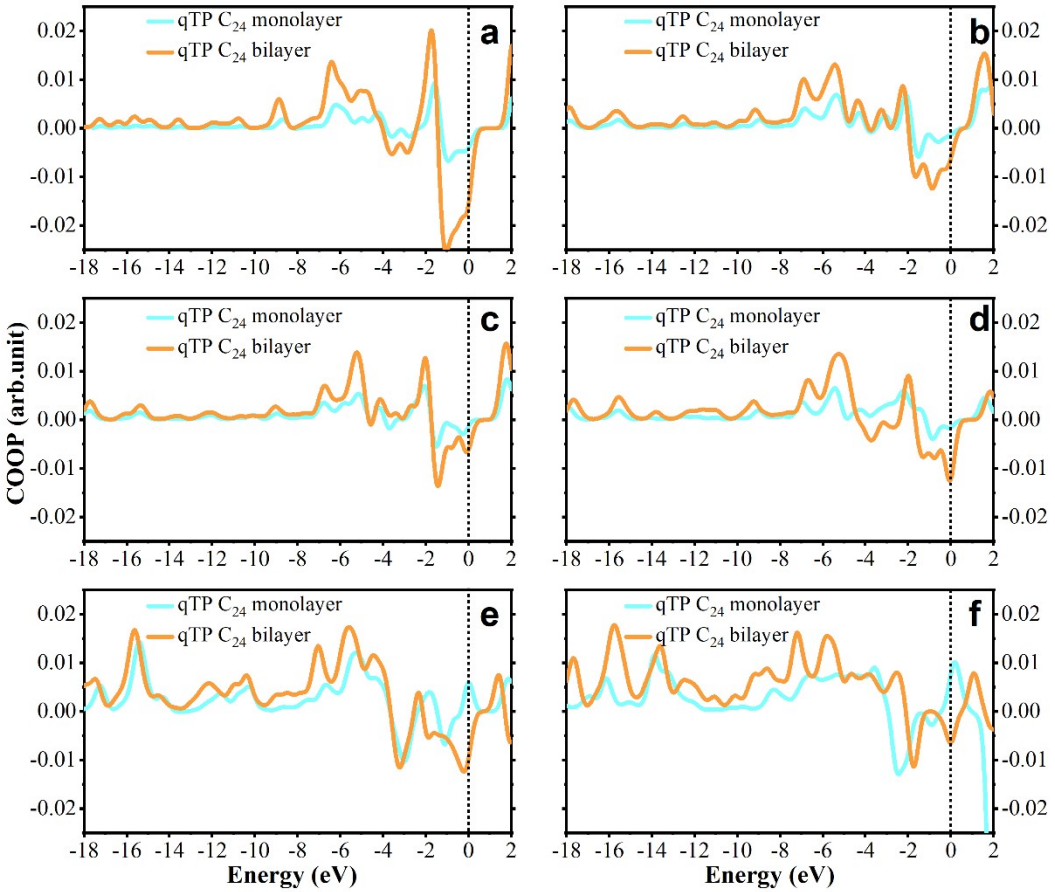


Figure S13. COOP plots of the qTP $C_{24}$ monolayer and bilayer with adsorptions of $S_8$ (a), $Li_2S_8$ (b), $Li_2S_6$ (c), $Li_2S_4$ (d), $Li_2S_2$ (e), $Li_2S$ (f), positive and negative values represent bonding and antibonding interactions between two fragments.

Table S2. Collected $\Delta G$ values associated with rate-limiting step for 2D monolayers reported previously.

| Substrates | $\Delta G_{max}$ (eV) |
|---|---|
| N–doped graphene[2] | 1.21 |
| $C_2N$[3] | 0.89 |
| Metal-decorated g-$C_3N_4$[4] | 0.49-1.37 |
| $MoS_2$[5] | 0.77 |
| $In_2Se_3$[6] | 0.77 |
| $V_2NF_2$[7] | 2.14 |
| $Fe_3GeTe_2$[8] | 0.41 |
| 1T′-$MoTe_2$[9] | 0.97 |
| (Sc, Ti, and V)-doped BP monolayers[10] | 0.61-0.88 |
| $MA_2Z_4$ monolayers[11] | 0.48-0.73 |
| $C_{60}$ monolayers[12] | 0.51-0.95 |

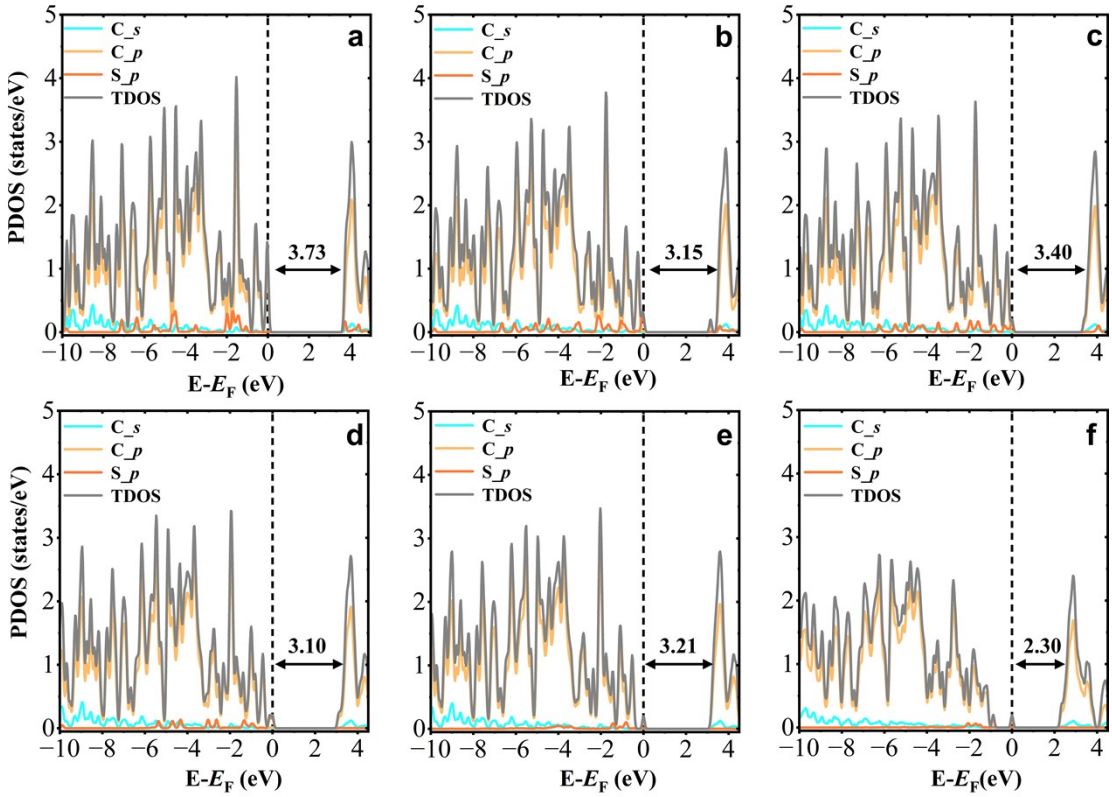


Figure S14. Projected density of states (PDOS) of qTP $C_{24}$ monolayer with adsorptions of $S_8$ (a), $Li_2S_8$ (b), $Li_2S_6$ (c), $Li_2S_4$ (d), $Li_2S_2$ (e), $Li_2S$ (f). The Fermi level is indicated with a dashed line.

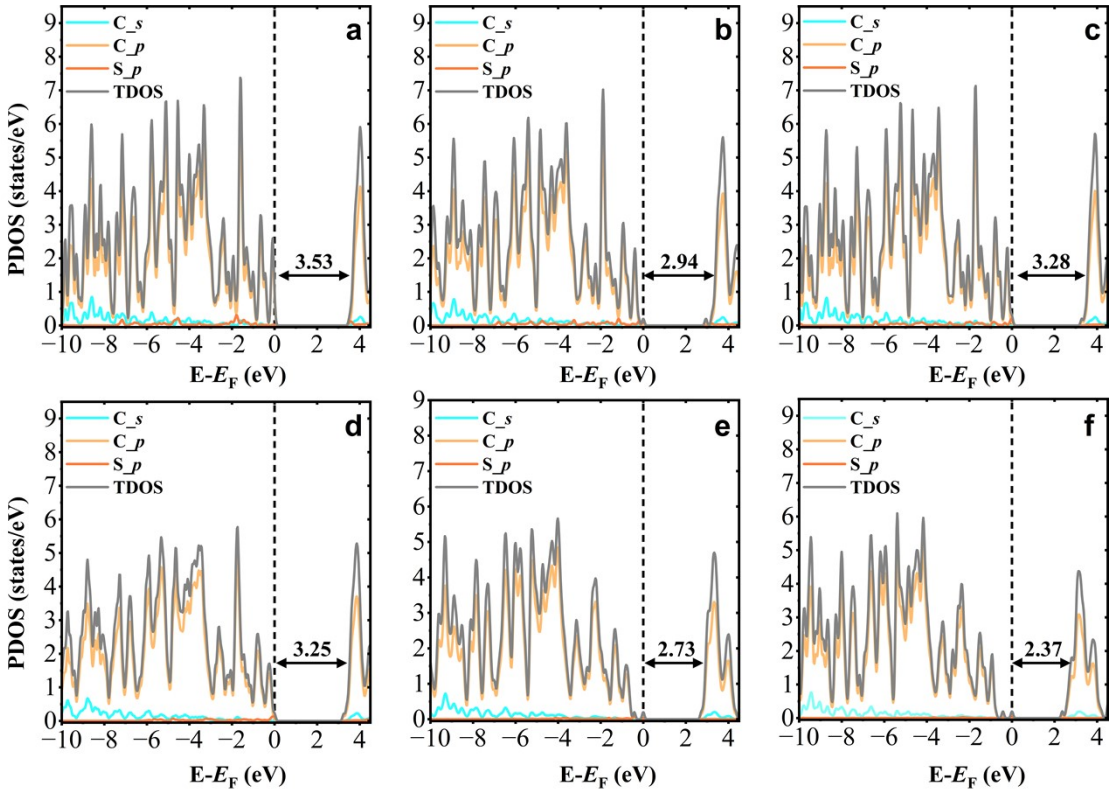


Figure S15. Projected density of states (PDOS) of qTP $C_{24}$ bilayer with adsorptions of $S_8$ (a), $Li_2S_8$ (b), $Li_2S_6$ (c), $Li_2S_4$ (d), $Li_2S_2$ (e), $Li_2S$ (f). The Fermi level is indicated with a dashed line.

## References


(1) Wu, J.; Peng, B. Smallest [5,6]Fullerene as Building Blocks for 2D Networks with Superior Stability and Enhanced Photocatalytic Performance. *J. Am. Chem. Soc.* **2025**, *147* (2), 1749–1757. https://doi.org/10.1021/jacs.4c13167.

(2) Zhang, L.; Liu, D.; Muhammad, Z.; Wan, F.; Xie, W.; Wang, Y.; Song, L.; Niu, Z.; Chen, J. Single Nickel Atoms on Nitrogen-Doped Graphene Enabling Enhanced Kinetics of Lithium–Sulfur Batteries. *Adv. Mater.* **2019**.

(3) Liang, Z.; Yang, D.; Tang, P.; Zhang, C.; Jacas Biendicho, J.; Zhang, Y.; Llorca, J.; Wang, X.; Li, J.; Heggen, M.; David, J.; Dunin-Borkowski, R. E.; Zhou, Y.; Morante, J. R.; Cabot, A.; Arbiol, J. Atomically Dispersed Fe in a $C_2N$ Based Catalyst as a Sulfur Host for Efficient Lithium–Sulfur Batteries. *Advanced Energy Materials* **2021**, *11* (5). https://doi.org/10.1002/aenm.202003507.

(4) Song, X.; Tian, D.; Qiu, Y.; Sun, X.; Jiang, B.; Zhao, C.; Zhang, Y.; Fan, L.; Zhang, N. Improving Poisoning Resistance of Electrocatalysts via Alloying Strategy for High-Performance Lithium-Sulfur Batteries. *Energy Storage Materials* **2021**, *41*, 248–254. https://doi.org/10.1016/j.ensm.2021.05.028.

(5) Shao, Q.; Lu, P.; Xu, L.; Guo, D.; Gao, J.; Wu, Z.-S.; Chen, J. Rational Design of MoS2 Nanosheets Decorated on Mesoporous Hollow Carbon Spheres as a Dual-Functional Accelerator in Sulfur Cathode for Advanced Pouch-Type Li–S Batteries. *Journal of Energy*

*Chemistry* **2020**, *51*, 262–271. https://doi.org/10.1016/j.jechem.2020.03.035.

(6) Yuan, H.; Zhang, Y.-W. Role of Ferroelectric $In_2Se_3$ in Polysulfide Shuttling and Charging/Discharging Kinetics in Lithium/Sodium–Sulfur Batteries. *ACS Appl. Mater. Interfaces* **2022**, *14* (14), 16178–16184. https://doi.org/10.1021/acsami.1c24801.

(7) Fan, K. Nitride MXenes as Sulfur Hosts for Thermodynamic and Kinetic Suppression of Polysulfide Shuttling: A Computational Study.

(8) Song, X.; Qu, Y.; Zhao, L.; Zhao, M. Monolayer $Fe_3GeX_2$ (X = S, Se, and Te) as Highly Efficient Electrocatalysts for Lithium–Sulfur Batteries. *ACS Appl. Mater. Interfaces* **2021**, *13* (10), 11845–11851. https://doi.org/10.1021/acsami.0c21136.

(9) Yu, B.; Huang, A.; Srinivas, K.; Zhang, X.; Ma, F.; Wang, X.; Chen, D.; Wang, B.; Zhang, W.; Wang, Z.; He, J.; Chen, Y. Outstanding Catalytic Effects of 1T′-$MoTe_2$ Quantum Dots@3D Graphene in Shuttle-Free Li–S Batteries. *ACS Nano* **2021**, *15* (8), 13279–13288. https://doi.org/10.1021/acsnano.1c03011.

(10) Jia, X.; Bai, L.; Zhang, M.; Niu, L. Transition Metal-Doped Boron Phosphide Monolayer in Lithium–Sulfur Batteries with Anchoring Ability and Catalytic Performance: A First-Principles Study. *J. Phys. Chem. C* **2023**, *127* (40), 19963–19972. https://doi.org/10.1021/acs.jpcc.3c03997.

(11) Du, J.; Zhou, X.; Cheng, X.; Jiang, G. Theoretical Evaluation of Monolayer MA2Z4 (M = Ti, Zr, or Hf; A = Si or Ge; and Z = P or As) Family as Promising Candidates for Lithium–Sulfur Batteries. *Journal of Colloid and Interface Science* **2025**, *678*, 150–158. https://doi.org/10.1016/j.jcis.2024.09.106.

(12) Du, J.; Shi, M.; Zhou, X.; Cheng, X.; Cheng, K.; Jiang, G. Monolayer Fullerene Networks for High-Performance Lithium–Sulfur and Sodium–Sulfur Batteries. *ACS Catal.* **2025**, *15* (11), 9949–9961. https://doi.org/10.1021/acscatal.4c07268.